Available online at www.sciencedirect.com
SCIENCE DIRECT
Earth and Planetary Science Letters 241 (2006) 202–210
EPSL
www.elsevier.com/locate/epsl

Plume heat flow is much lower than CMB heat flow

Eric Mittelstaedt [a,*], Paul J. Tackley [a,b]

[a] Department of Earth and Space Sciences, University of California, Los Angeles, USA
[b] Institute of Geophysics and Planetary Physics, University of California Los Angeles, USA

Received 13 September 2004; received in revised form 5 September 2005; accepted 2 October 2005
Available online 21 November 2005
Editor: Scott King

Abstract

Plumes rising from the core–mantle boundary (CMB) are often assumed to transport most, or all, of the heat conducted across the CMB. Here this assumption is explored using numerical convection models in idealized geometries that lead to a single plume under steady-state or near steady state conditions. Plume heat transport is calculated for different internal heating rates using two methods and compared to the CMB heat flux. For these conditions, it is found that the heat flux transported by plumes in the upper mantle is only a fraction of the core heat flux and, thus, core heat flow estimates derived from observed hotspots could be multiplied by a factor of several.

Keywords: mantle convection; plumes; heat flow; core mantle boundary; hotspot

1. Introduction

Hotspots such as Iceland and the Hawaiian Islands are commonly believed to be formed by long-lived plumes that arise from a thermal boundary layer above the core–mantle boundary (CMB) [1–4]. Based on the topographic uplift observed above known hotspots, G.F. Davies [5] estimated that plumes carry 6% of the mantle heat flux, or 12% when starting plume heads causing flood basalts [6] are included. Such estimates of plume heat flux have led to the 'standard' mantle model in which 80–90% of mantle heat loss is associated with oceanic plate cooling and subduction of cold lithosphere, while the rest is associated with plumes.

As plumes are commonly assumed to originate from just above the CMB, it is often assumed that the heat flux carried by observed plumes is equal to the heat flux through the CMB; in other words, plumes cool the core while slabs cool the mantle [7]. However, it seems likely that other heat loss mechanisms will be present at the CMB. The basic dynamics of convection suggest one: in a simple, basally heated isoviscous 2-D convection cell, the upwelling ('plume') carries only 50% of the basal heat flow, the other 50% being used to warm the cold limb that spreads across the boundary. Translated to the Earth, this corresponds to "slab warming", i.e., warming of cold slabs that spread above the CMB from colder than the mantle adiabat to the mantle adiabat, and this might be accentuated due to the CMB being much smaller in surface area than the surface. Another 'invisible' core heat loss mechanism was proposed by Malamud and Turcotte [8], who, by adding in contributions from 5200 unseen 'stealth' plumes that were assumed to follow a power-law size distribution, estimated a plume heat flux as high as 35% of surface heat flux; these unseen plumes would transfer core heat into the

* Corresponding author. Present address: Department of Geology and Geophysics, University of Hawaii at Manoa, USA.
E-mail address: staggle@soest.hawaii.edu (E. Mittelstaedt).

0012-821X/$ - see front matter © 2005 Elsevier B.V. All rights reserved.
doi:10.1016/j.epsl.2005.10.012

general mantle. Finally, Jellinek et al. [9] proposed added core cooling due to rapid lateral advection of the CMB boundary layer by mantle flow.

To investigate such matters, [10] presented an isoviscous 3-D numerical experiment heated 50% from within and 50% from below in which upwellings and downwellings were detected and their heat transport calculated. This experiment found that (i) downwellings induce upwellings from the lower boundary (evident visually and from time series of heat flux), (ii) the heat transported by upwelling plumes is a small fraction of the CMB heat flow (between 1/5 and 1/10 depending on how measured), and (iii) a majority (~2/3) of starting hot plumes do not reach the top boundary layer. These results support the 'slab warming' and 'stealth plume' models of heat transport. However, the mantle model assumed in that study did not include depth- and temperature-dependent viscosity, commonly thought to be important in the dynamics of mantle convection. Additionally, only one set of parameters was considered. Thus, we here present numerical experiments to determine the effect of viscosity variations and a systematic variation of the internal heating rate (hence ratio of internal to basal heating) on plume heat transport [11]. A simplified, two-dimensional geometry that results in a single plume is used for easier study.

2. Model

Calculations are performed in two-dimensional geometry. In addition to a Cartesian layer, axisymmetric geometry is considered so that a columnar rather than linear plume is obtained; both have an aspect ratio of unity. To investigate the effect of differing CMB and outer surface areas, cylindrical geometry is also considered, with the domain spanning an angle of 0.6 radians (rad) to give approximately the same domain width as the Cartesian cases. The horizontal boundaries are isothermal, free slip and impermeable, and the vertical boundaries are reflecting, as is usual for calculations in a fairly small domain. Both constant-viscosity and temperature- and depth-dependent viscosity cases are considered.

The usual non-dimensional equations of thermal convection in an incompressible Boussinesq fluid with infinite Prandtl number are used. These are, conservation of mass

$$\nabla \cdot \vec{v} = 0 \tag{1}$$

conservation of momentum,

$$\nabla \cdot \left(\eta\left(v_{i,j} + v_{j,i}\right)\right) - \nabla p = RaT\hat{z} \tag{2}$$

where the Rayleigh number, Ra, is

$$Ra = \frac{\rho g \alpha \Delta T D^3}{\eta \kappa} \tag{3}$$

and conservation of energy

$$\frac{\partial T}{\partial t} = \nabla^2 T - \vec{v} \cdot \nabla T + h \tag{4}$$

where $\vec{v}$, p, T, ρ, κ, α, and η are velocity, dynamic pressure, temperature, density, thermal diffusivity, thermal expansivity and dynamic viscosity. The internal heating rate, h, is given by:

$$h = \frac{HD^2}{k\Delta T} \tag{5}$$

where H is the volumetric heating rate and k is the thermal conductivity. h is varied between 0 and 20. For simplicity, phase changes are not included.

The viscosity is assumed to be either constant, or dependent on temperature and depth. Viscosity can vary due to temperature by up to a factor of 1000 and due to depth by up to a factor of 10, i.e.,

$$\eta(T,z) = \exp[V_1(T - 0.5) + V_2(0.5 - z)] \tag{6}$$

where $V_1 = 6.907$ (but is varied in one series of runs) and $V_2 = 2.302$.

The equations are discretized and solved using STAG3D [12], a primitive-variable, finite-volume multigrid solver. The numerical resolution is 64 by 64 cells with vertical grid refinement near the upper and lower boundaries. Tests indicate that this resolution is sufficient for capturing the heat flow characteristics at the given Rayleigh numbers. Doubling the number of points in each direction produces a change of 0.3–2.3% in the heat flux and 1.6–3% in the difference between surface and near surface heat flux (Fig. 1).

Cases are run until they reach a steady state or statistically steady-state (i.e., with some slight time dependence but no secular trend). The reference Rayleigh number (defined using the viscosity at mid-temperature and mid-depth) is limited to 10^6 due to the extended time required to achieved statistically steady-state solutions at higher Ra, as previously noted in 3-D [13], although in one series of runs Ra of up to 5×10^6 are considered.

3. Calculating heat transport

Boundary heat fluxes are straightforward to calculate, with the complexity, that in cylindrical geometry

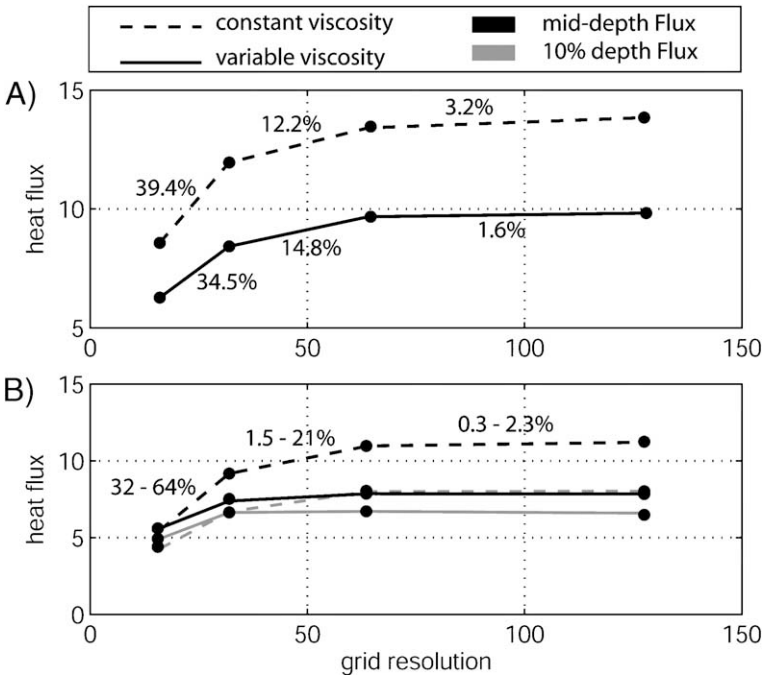

Fig. 1. The difference between surface and near-surface (10% depth) heat flux (A) and values of the heat flux at mid-depth and 10% depth (B) versus resolution for both constant and variable viscosity cases without internal heating.

heat flow/rad, rather than heat flux (per unit area), is used so that CMB and surface values are directly comparable. Away from boundaries, heat transport by upwellings and downwellings is computed by horizontally integrating the product of temperature anomaly (relative to the horizontally averaged temperature) with vertical velocity, using two different methods.

In Method A, the calculation of upwelling flux is performed over material that is moving upwards and has a temperature that is higher than the horizontal average (to exclude the contribution of material that is dragged in the 'wrong' direction), i.e.,

$$F_{\mathrm{up}}(z) = \int \max[v_z,0]\max\left[T-\bar{T},0\right]\mathrm{d}x$$

with an analogous definition for downwelling flux:

$$F_{\mathrm{dn}}(z) = \int \min[v_z,0]\min\left[T-\bar{T},0\right]\mathrm{d}x$$

where F_{up} and F_{dn} are heat flows carried by upwellings and downwellings respectively, and $\bar{T}$ is the instantaneous horizontally averaged temperature. This method measures the total upward or downward advected flux, but is not good for identifying fluxes for individual features such as plumes or slabs. For example, the pervasive hot upwelling flow that is characteristic of predominantly internally heated convection would be included in the integration of upwelling flux, but is not something that would be identified as 'plume' related based on its surface expression. Thus, Method A leads to an upper bound on the 'plume' heat flux.

The second method used in the Cartesian and axisymmetric cases, Method B, attempts to limit the integration to features that can be clearly identified as plumes based on their temperature anomaly, following the method of Labrosse [10]. Material is considered to be part of a plume if its temperature anomaly exceeds a threshold based on the total range of variation at that depth, i.e., if

$$T-\bar{T} \geq a\left(T_{\max}-\bar{T}\right)$$

where $T_{\max}$ is the instantaneous maximum temperature at that depth, and a is a constant discussed below. The heat flux carried by hot plumes is then given by:

$$F_{\mathrm{up}}(z) = \int \max[v_z,0]\max\left[T-\bar{T},0\right]H\left[T-(1-a)\bar{T} - aT_{\max}\right]\mathrm{d}x$$

which is similar to the Method A formula except that the Heaviside function H limits the integration to material that has at least the specified temperature anomaly (i.e., Method A is the same as this but with $a=0$).

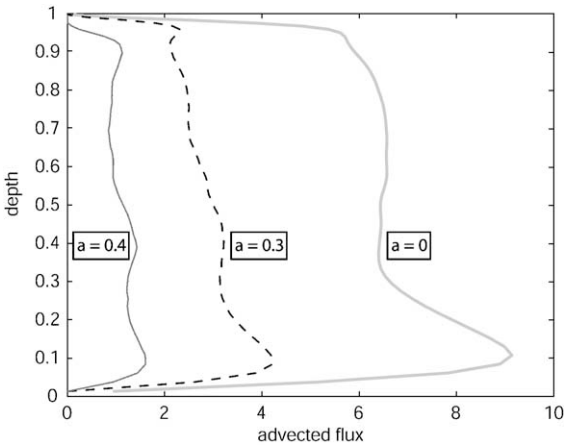

Fig. 2. Advected flux versus depth for Method B threshold choices of $a=0.4$ (thin grey line), $a=0.3$ (dashed line), and $a=0$ (thick grey line) illustrates the choice of 0.3.

Values for the constant a between 0.2 and 0.5 were tested, but extreme values were found to give anomalously large or truncated fluxes, especially near the top and bottom boundaries (Fig. 2). A value of 0.3 gives a good compromise and it was chosen for the present study. Method B thus eliminates the contribution of upwellings and downwellings that do not have a distinct temperature anomaly. However, it has the disadvantage that sometimes a genuine plume's temperature anomaly falls below (i.e. is cooler than) the threshold value. Thus, Method B gives a lower bound to the plume heat flux.

In summary, the two Methods A and B are considered to give upper and lower bounds of the plume heat flux measurements, and are compared in the analysis that follows.

4. Results

4.1. Temperature fields

Representative temperature fields for different scenarios and internal heating rates of 0 or 10 are illustrated in Fig. 3. In all cases, a single upwelling is obtained, which is at the axis in axisymmetric cases, while a downwelling exists at the other side of the box. In some cases, small-scale instabilities are superimposed on the large-scale structure. Naturally, internal heating leads to a higher internal temperature and a lower temperature contrast between the plume and the surrounding mantle, such that in the non-axisymmetric cases the plume is very faint in the upper part of the mantle. In axisymmetric geometry the plumes are wider and maintain a clear thermal signature throughout the mantle.

4.2. Temperature profiles

Time averaged temperature profiles of horizontal mean, minimum and maximum temperature (Fig. 4) show clearly the cold and hot thermal boundary layers at top and bottom, and a local cold anomaly just above the lower boundary layer that is caused by spreading of the downwelling above the boundary. In some cases, particularly those with no internal heating, a local hot anomaly is also visible just below the cold upper boundary layer. The minimum and maximum temperatures are important here because they are used in the algorithm to calculate plume heat transport. They are more strongly depth-dependent than the mean temperature due to lateral diffusion of heat, as an upwelling or

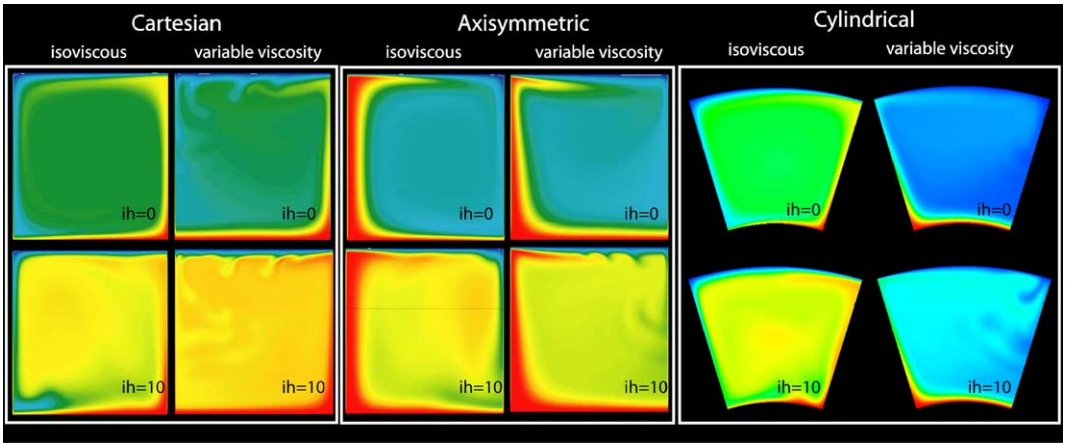

Fig. 3. Temperature fields for cases with internal heating of zero (top row) or 10 (bottom row) in the three geometries: Cartesian (left panel), Cartesian axisymmetric (center panel) and cylindrical (right panel). Within each panel, the cases on the left are isoviscous and the ones on the right have variable viscosity.

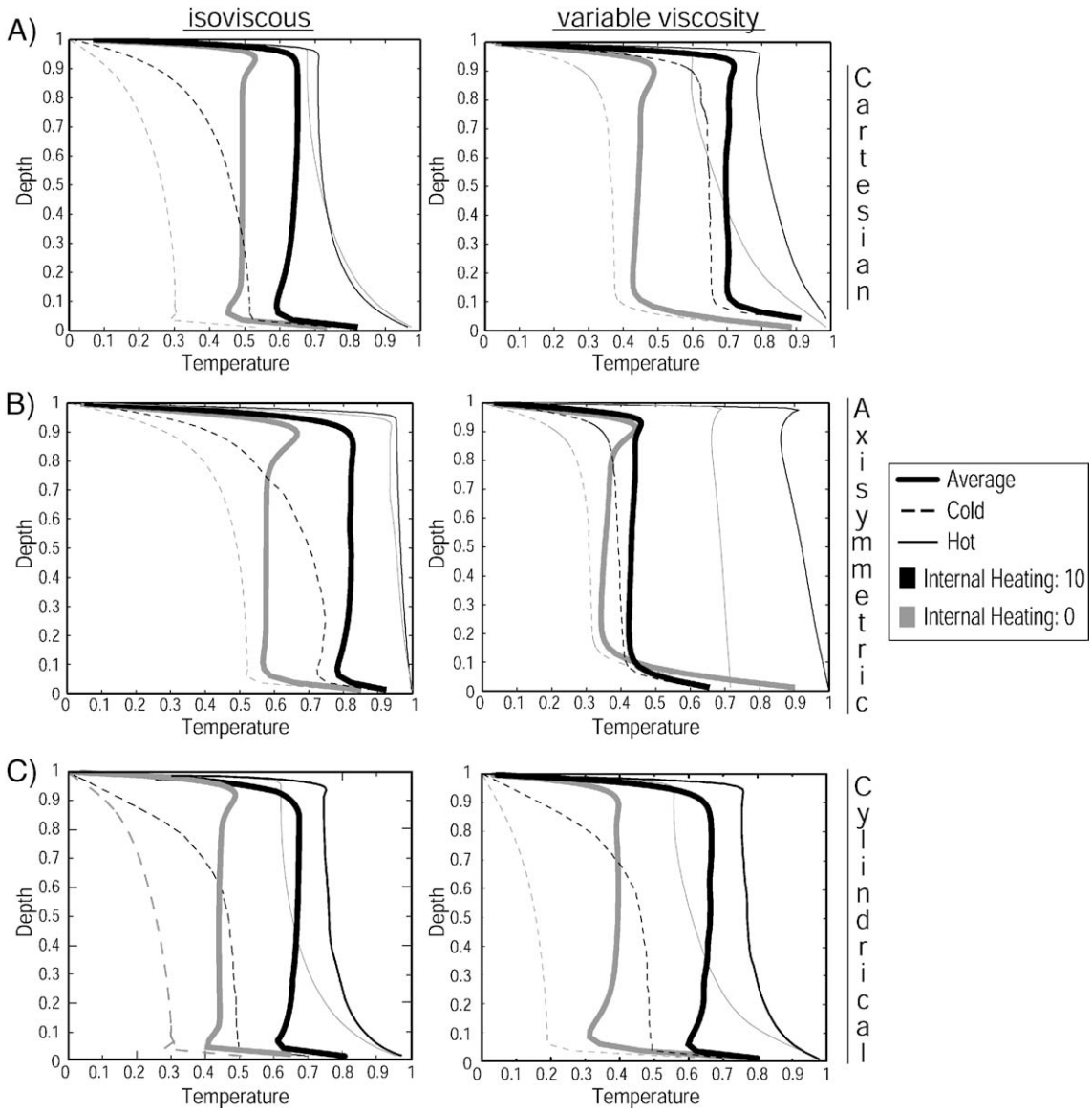

Fig. 4. Vertical profiles of horizontally averaged temperature (thick lines), maximum temperature (thin lines) and minimum temperature (dashed lines) for cases with an internal heating rate of zero (black lines) or 10 (gray lines). (A) Cartesian geometry; (B) axisymmetric geometry; (C) cylindrical geometry.

downwelling traverses the domain. The maximum temperature, which occurs at the center of the plumes, decreases rapidly as the plume rises; less rapidly in axisymmetric cases.

4.3. Flux vs. depth

Fig. 5 compares time averaged total, hot and cold advected fluxes versus depth for cases with an internal heating rate of 10 in all three geometries and with constant and variable viscosity and both Methods A and B. Due to time variation of the flow and the finite averaging period, the profiles are often not perfectly smooth. The advected flux is zero at the boundaries because the vertical velocity goes to zero and forces conductive heat transport, and in the interior it increases approximately linearly with height due to internal heating. The extrapolation of this linear trend to the boundaries corresponds to the boundary heat flux.

Typically, the upwelling flux is roughly constant with depth, though in some cases is higher near the

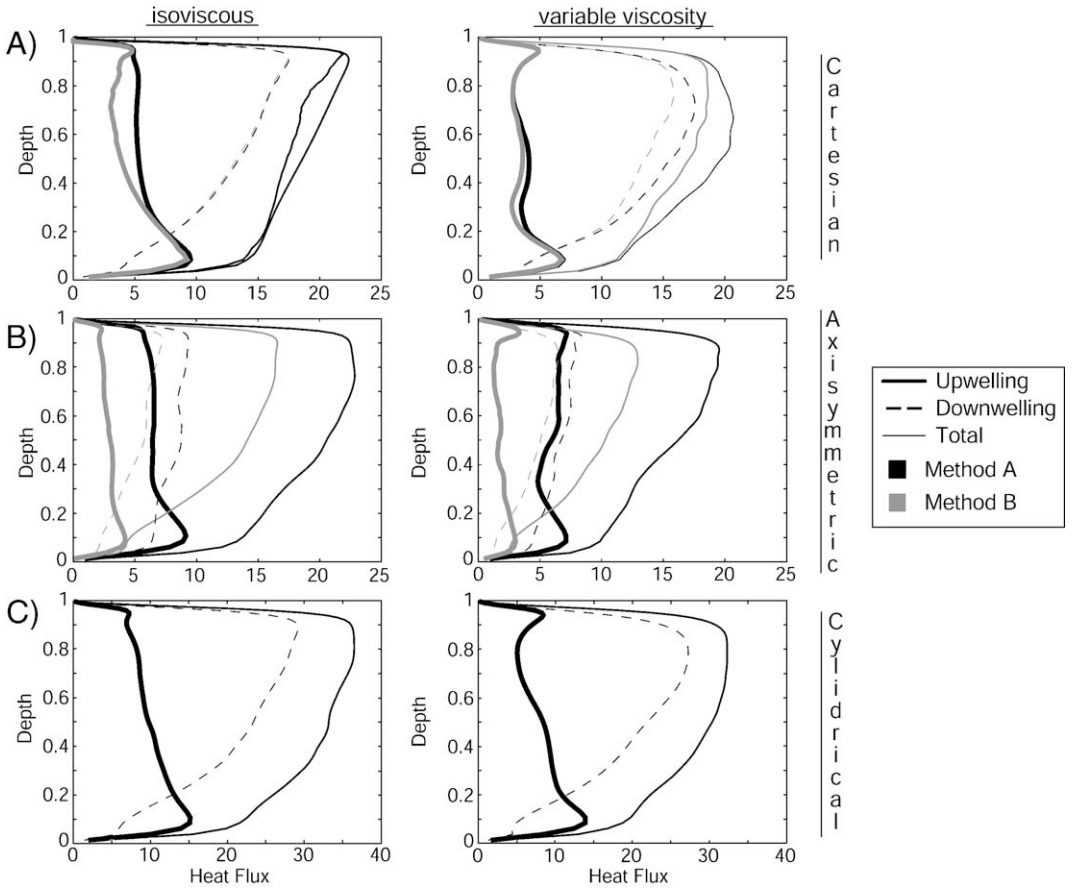

Fig. 5. Vertical profiles for cases with an internal heating rate of 10 of upwelling heat flux (thick lines), downwelling heat flux (dashed lines) and total advected heat flux (thin lines) using Method A (black lines) and Method B (gray lines). (A) Cartesian; (B) axisymmetric; (C) cylindrical.

bottom due to the decrease in mean temperature in this region. In contrast, the downwelling flux increases with height, which is due to the contribution of internal heating (10 in these cases) to the geotherm. In all cases, the heat transport by downwellings exceeds that by upwellings, but the difference is much smaller with axisymmetric geometries. In isoviscous cases with no internal heating (not plotted here) there is symmetry between upwellings and downwellings. The profiles are similar in all three geometries, suggesting that these findings are robust.

The calculated heat fluxes are always lower with Method B due to the fact that temperature anomalies must exceed a given threshold in order to be counted, emulating the process used by humans to identify hot, upwelling plumes from surface observations. The amount of reduction ranges from very small (as in the isoviscous Cartesian cases) to approximately 50% (e.g., the axisymmetric cases). Often, the reduction in upwelling flux is larger than the reduction in downwelling flux (e.g., the axisymmetric cases).

4.4. Plume flux vs. reference Rayleigh number

The CMB heat flux is compared to the mid-depth upwelling plume flux in Fig. 6A. The cases shown are temperature- and depth-dependent without internal heating. The Rayleigh number is varied from 10^4 to 5×10^6.

Both the upwelling plume flux and the CMB flux increase with larger Rayleigh number with the CMB flux increasing slightly more rapidly. The fraction of core heat flux carried by plumes decreases slightly with increasing Rayleigh number.

4.5. Plume flux vs. viscosity dependence (V_1)

The variation of upwelling and downwelling heat flux at mid-depth is examined at different values of temperature dependence of the viscosity in Fig. 6B. Fluxes are calculated using a Cartesian model with no internal heating and a fixed dependence of viscosity on depth.

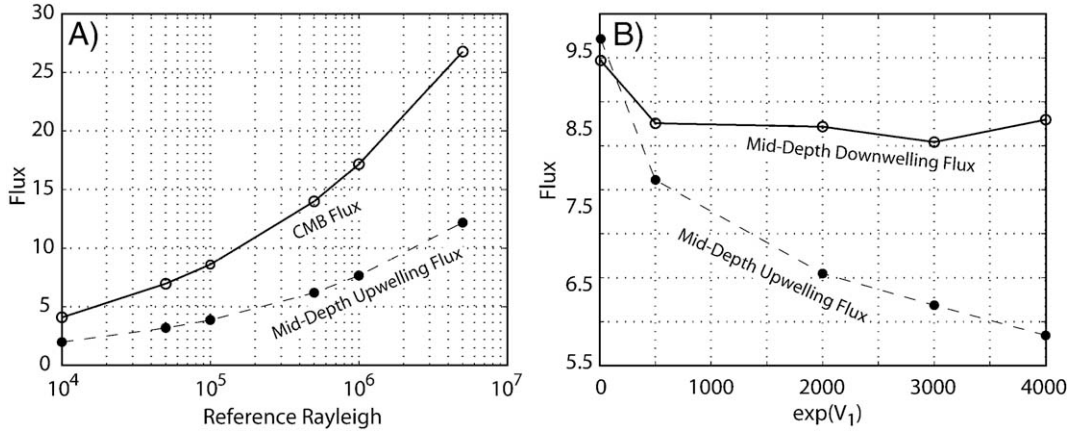

Fig. 6. Upwelling flux measurements versus values of the reference Rayleigh number (A) and V_1 (B).

Increasing the temperature dependence of viscosity by ~2.5 orders of magnitude decreases the upwelling flux transported by plumes by half, but no significant change in downwelling flux is evident. In other words, at higher values of V_1 downwellings dominate heat transport.

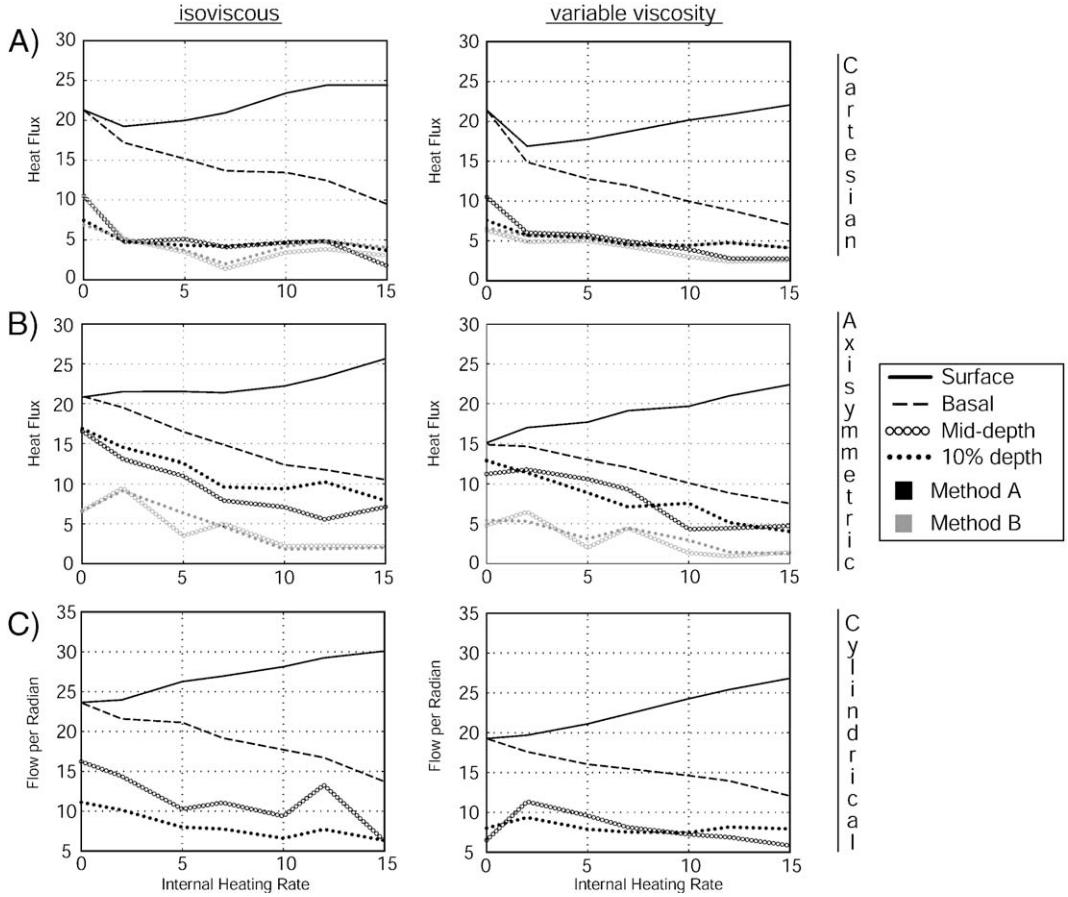

Fig. 7. Heat fluxes at various depths as a function of internal heating rate: surface (thick lines), basal (dashed lines), mid-depth advected (circled lines) and 10% depth advected (dotted lines) using Method A (black lines), and Method B (gray lines). (A) Cartesian; (B) axisymmetric; (C) cylindrical.

4.6. Plume flux vs. internal heating

The heat flux carried by upwellings is compared to basal and surface fluxes for varying internal heating rate and all scenarios in Fig. 7. Upwelling flux is calculated at either mid-mantle depth or, more relevant for surface observations, 10% depth (300 km).

The upper lines in each graph show the surface and basal heat fluxes, which differ by an amount equal to the internal heating rate, while the small-dotted lines show the upper mantle (300 km depth) upwelling heat flux. The focus here is on how upwelling flux compares to the CMB heat flux, and the first-order observation is that it is generally substantially lower, particularly when the plume flux at 10% (300 km) depth is considered. For example, for the cases illustrated in Fig. 3 with $H=10$, the upwelling heat flux at 300 km depth calculated with Method A is typically about 50% of the CMB heat flux but can be as low as ~10% (isoviscous Cartesian) or as high as 75% (variable viscosity axisymmetric). Using Method B, it is always lower than ~40% of CMB heat flux.

At other heating rates the upwelling heat flux is relatively constant or decreases slightly with internal heating rate, the exception being for isoviscous cases between $H=0$ and $H=5$. In any case, above $H=5$, this means that upwelling heat flux represents an increasingly larger fraction of basal heat flux as H is increased. While this may seem odd, it is related to the heat input into the mantle by internal heating, which contributes to a broad upwelling flow that is included when using Method A. Even in Method B, the difference between mantle geotherm and maximum temperature decreases, so a smaller temperature anomaly will be counted as a 'plume'. However, at very high internal heating rates, there are no 'plumes' that can be identified based on their thermal anomaly, so the results of this modeling should not be taken literally. Requiring an absolute temperature anomaly, rather than one that scales with the difference between the geotherm and maximum temperature, might eliminate spurious measurement of general hot background upflow as upwelling flux of 'plumes'.

5. Discussion and conclusions

Differences in plume heat flux and CMB heat flux in the above cases suggest that a sizable "unseen" flux is being transported out of the core by methods other than hot upwelling plumes. If the calculation of upwelling heat flux is limited to those features with a distinct temperature anomaly then the difference is particularly pronounced. In the simple cases presented, this "unseen" flux is mostly due to warming of cold downwellings that settle above the CMB [16], analogous to "slab warming" rather than the other two proposed mechanisms "stealth plumes" [8] or "advection by large-scale flow" [9]. That this mode operates in the Earth is evidenced by the consistent tomographic imaging of cold slabs in the deep mantle (e.g., Grand et al. [14] and van der Hilst et al. [15] summarized in Steinberger [16]) while imaging of hot plumes requires special processing [17]. In addition to upwellings initiated at the CMB, upwellings may also develop from a possible boundary layer between the upper and lower mantles, but this study is restricted to examining core heat loss by whole mantle convection. For a predominantly internally heated mantle, as thought to be appropriate for Earth, convection is dominated by downwellings, which may therefore exert a greater control over the amount of heat coming from the core than upwellings [10].

Higher values of the Rayleigh number lead to lower fractions of the CMB flux being carried by upwelling plumes. This implies that the amount of heat carried away from the core by plumes may be even less than suggested here.

These conclusions are relatively insensitive to geometry (Cartesian, axisymmetric or cylindrical), although the quantitative numbers differ. In axisymmetric geometry, where plumes are, most realistically, columnar, the fraction of core heat flux that they carry is lowest, although they retain a higher fraction of their temperature anomaly as they travel through the mantle. In cylindrical geometry, where the CMB has a smaller area than the outer boundary, the results are only slightly different from Cartesian geometry.

It has been suggested that variable thermal conductivity may lead to a low conductivity zone near the surface of the Earth that inhibits heat flow. Our measurements of heat flux are all well within the mantle and would not be effected by these processes.

The presented models are greatly simplified relative to the real Earth for easier analysis; however, in the future, such analysis must be carried out for more realistic models that incorporate three-dimensional, plate-like behavior at the surface and realistic convective vigor.

Acknowledgments

The authors thank Stéphane Labrosse for advice and suggestions, and Jeroen van Hunen and an anon-

ymous reviewer for constructive reviews. Funded by the David and Lucile Packard Foundation and NSF grant EAR-022950.

References

[1] W.J. Morgan, Convection plumes in the lower mantle, Nature 230 (1971) 42–43.
[2] B. Steinberger, Plumes in a convecting mantle: models and observations for individual hotspots, J. Geophys. Res. 105 (B5) (2000) 11127–11152.
[3] F.D. Stacey, D.E. Loper, The thermal-boundary-layer interpretation of D″ and role as a plume source, Phys. Earth Planet. Inter. 33 (1) (1983) 45–55.
[4] D.E. Loper, F.D. Stacey, The dynamical and thermal structure of deep mantle plumes, Phys. Earth Planet. Inter. 33 (4) (1983) 304–317.
[5] G.F. Davies, Ocean bathymetry and mantle convection: 1. Large-scale flow and hotspots, J. Geophys. Res. Solid Earth Planets 93 (B9) (1988) 10467–10480.
[6] I.H. Campbell, R.W. Griffiths, Implications of mantle plume structure for the evolution of flood basalts, Earth Planet. Sci. Lett. 99 (1–2) (1990) 79–93.
[7] G.F. Davies, M.A. Richards, Mantle convection, J. Geol. 100 (2) (1992) 151–206.
[8] B.D. Malamud, D.L. Turcotte, How many plumes are there?, Earth Planet. Sci. Lett. 174 (1–2) (1999) 113–124.
[9] A.M. Jellinek, H.M. Gonnerman, M.A. Richards, Plume capture by divergent plate motions: implications for the distribution of hotspots, geochemistry of mid-ocean ridge basalts and estimates of the heat flux at the core–mantle boundary, Earth Planet. Sci. Lett. 205 (2003) 361–378.
[10] S. Labrosse, Hotspots, mantle plumes and core heat loss, Earth Planet. Sci. Lett. 199 (2002) 147–156.
[11] E.L. Mittelstaedt, P.J. Tackley, Plume heat flow is much less than CMB heat flow, EOS Trans. AGU, Fall Meeting Suppl. 82 (47) (2001) F1133–F1134.
[12] P.J. Tackley, Effects of strongly variable viscosity on three-dimensional compressible convection in planetary mantles, J. Geophys. Res. 101 (1996) 3311–3332.
[13] C. Sotin, S. Labrosse, Three-dimensional thermal convection in an iso-viscous, infinite Prandtl number fluid heated from within and from below: applications to the transfer of heat through planetary mantles, Phys. Earth Planet. Inter. (Netherlands) 112 (3–4) (1999) 171–190.
[14] S.P. Grand, R.D. van der Hilst, S. Widiyantoro, Global seismic tomography: a snapshot of convection in the Earth, GSA Today 7 (4) (1997) 1–7.
[15] R.D. van der Hilst, S. Widlyantoro, E.R. Engdahl, Evidence for deep mantle circulation from global tomography, Nature 386 (6625) (1997) 578–584.
[16] B. Steinberger, Slabs in the lower mantle — results of dynamic modelling compared with tomographic images and the geoid, Phys. Earth Planet. Inter. 118 (3–4) (2000) 241–257.
[17] R. Montelli, G. Nolet, F.A. Dahlen, G. Masters, E.R. Engdahl, S.H. Hung, Finite-frequency tomography reveals a variety of plumes in the mantle, Science 303 (5656) (2004) 338–343.